

MONITORING ROLLING ELEMENT BEARINGS USING FIBER OPTIC ROLLING ELEMENT SENSING TECHNOLOGY (FOREST)

Andrew P. Conkey,

Department of Mechanical Engineering
3123 F1/2, Texas A&M University
College Station, TX 77843
Tel: (979) 847-9383; Fax: (979) 845-3081

Juan C. Juarez,

Department of Electrical Engineering
214 ZEC
3128 Texas A&M University
College Station, TX 77843

Tel.: (979) 696-8327, Fax: (979) 845-6259
jcj@tamu.edu

Henry F. Taylor

Department of Electrical Engineering
214 ZEC

3128-Texas A&M University
College Station, TX 77843

Tel: (979) 845-7563 FAX (979)845-6259
taylor@ee.tamu.edu

Abstract: Roller element bearing failures are often attributed to overload. Current vibration instrumentation is unable to provide information regarding static and dynamic loading. The authors have developed a transducer using the Fiber Fabry Perot Interferometer (FFPI) as a strain gage to acquire this previously unavailable information. The sensing element, which consists of two internal mirrors separated by a specified length of single mode optical fiber, offers a number of advantages over traditional transducers: high sensitivity (0.05 micro-strain), small diameter (4.9 mils, 0.125 mm), immunity to electromagnetic fields, and continuous operation at high temperatures (752 °F, 400 °C). Signals acquired from the Fiber Optic Rolling Element Sensing Technology (*FOREST*) sensor were processed to determine bearing frequency content and response to load changes, and the data was applied to detect bearing installation information. The sensors for these tests were mounted in the highly loaded zone of the bearing housings, in close proximity to the outer races. The results show that this fiber optic sensor can provide useful new information about bearing condition and loading in rotating machinery.

Key Words: roller bearings, loading, fiber optic, FFPI, time waveforms, spectrums, slow roll interferometer.

Introduction: A sensor has been developed to monitor the load in roller element bearings that incorporates the Fiber-Fabry-Perot-Interferometer (FFPI). This sensor reacts to the load that is developed in the housing of the bearing due to the passage of the rolling elements. The response of the sensor includes rotor system information as well as information concerning the loading of the bearing. Additionally, the sensor is capable of obtaining information at low speeds as well as change in static loads.

Review: The application of traditional means to monitor rolling element bearings is primarily for the detection of the onset of failure of the bearing. The information provided does not necessarily allow for diagnostic practices to be applied [1]. Although the failure of bearings before the expected life, L_{10} , is not uncommon as most predications can over predict the L_{10} by 14 % for ball bearing systems [2]. However, if a machine consistently fails, or is need for major design changes, the information regarding the loading of the bearings is not readily available from the current roller bearing monitoring practices [3]. The *FOREST* bearing sensor based on FFPI technology does allow for the capability of obtaining information on the loading of the bearing.

Roller bearings are a critical element in the rotor system as it is the bearing that maintains alignment of the rotor as well as to support the rotor. To perform this task, roller bearings are required to transfer all developed loads between the rotor and the housing. The loading on roller bearing system stems from static and dynamic loads. Static loads arise from interference fits, rotor dead load, misalignments, and drive pre-loads. Dynamic sources of loads are drive loads, process loads, and rotor loads. Although life factors are taken into account for many of these influences, most of the time they are a best guess approximation [4]. Although the results are generally conservative, a small percent of change in any one of the contributing loads can overcome any built in safety factor. As an example, a 15% change in the estimated radial load of a bearing can reduce the expected L_{10} by 35%. The ability to accurately predict the actual loads that are acting on a bearing is not possible. However, it is felt that the FFPI based sensor does have the ability to provide information regarding the loading on a bearing.

The loading on a bearing is critical as it also influences how well a rolling element tracks in the race. If a ball is not loaded sufficiently, it can have the tendency to skid. A skidding ball can break through the lubricating boundary layer and mar the race surface. Likewise, a ball that is heavily loaded may fail suddenly or generate excessive shear stresses in the race surface and cause failure. The dimensional differences that can occur in a bearing can cause these load variances. The grade of bearing does play a relevant factor in the variance of load from rolling element to the next rolling element. The higher the grade, the better the fit in tolerances between the rolling elements and the races and the higher the likelihood that each rolling element will experience an equal loading. A lower grade bearing can have significant deviations in rolling element diameter and race diameter which can lead to unequal loading of the rolling elements.

Sensor Background: The *FOREST* sensor consists of a single mode communication grade fiber with a set of imbedded di-electric mirrors that are separated by a fixed distance [5]. The variation of the spacing between the mirrors causes a phase shift to occur between the laser light returned by the mirror to that of a reference sensor that does not experience any change in mirror gap. The phase developed due to the displacement between the mirrors is converted into a digital signal using a signal conditioning unit (SCU)[6]. The fiber portion that contains the mirrors is embedded in a mandrel so that it can be inserted into the bearing housing. The design of the mandrel does dictate the relation between the developed strain between the mirrors and the load developed in the sensor assembly.

The application of sensors based on the FFPI principle can be found in studies involving the loading of railway structures [6], monitoring pressure of large reciprocating compressors [7], tilt pad bearings [8], magnetic bearings [9], and pump cavitations [10].

Roller Bearing Applications: The desire to monitor the trends of a roller element bearing at the outer race has been well established as strain gages, capacitive probes [11], eddy current probes [12], [13], piezoelectric chips [14], and reflected fiber optic systems [15], [16], [17] have all been used to observe how the outer race deflects due to the passage of a rolling element. Many of these analyses have demonstrated that the motion

of the outer race is constrained by the housing resulting in forces being exerted on the interior of the housing and that the passage of the rolling elements generates an observable motion. The *FOREST* sensor does not make contact with the outer race rather the tip of the *FOREST* sensor makes contact with about 15 mils of the housing material that is between the tip of the sensor and the outer race of the bearing, figure 1. The arrow in figure 1 emphasizes the material between the outer race of the bearing and the sensor tip. This strategy eliminates or reduces any undesired stresses that might act on the outer race of the bearing and the housing. In addition, if the outer race were to slip, the resulting motion would degrade the calibration setting of the sensors that monitor the displacement of the outer race. In this case, the *FOREST* sensor would not be affected. The information that the sensor provides is defined in terms of load and the calibration is not a function of the sensors relation to the outer race. The information from the *FOREST* sensor could be defined in terms of strain or displacement as well. This information could be used to relate the deflection of the sensor to the deflection of the components of the roller bearing. This type of analysis requires an extensive understanding of the bearing construction as well as an accurate model of the system. However, forces observed by the *FOREST* sensor can easily be related to the forces developed on the inner race by applying a transfer function relating the load observed by the sensor to a load applied to the shaft when the rolling element is directly in line with the sensor.

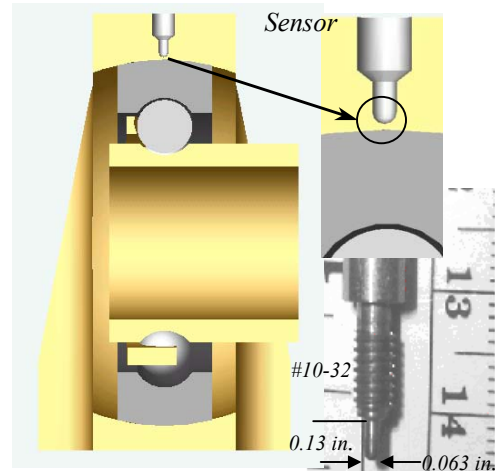


Figure 1: Exemplar sensor installation

Testing: Testing of the *FOREST* sensor was conducted using a rotor system supported by two 200 series pillow block bearings with ten balls, figure 2. The rotor is made of aluminum, and spans 90% of the distance between the two bearings, and weighs 14 lbs (6.36 kg). The rotor has a one-inch (25.4 mm) shaft that supports the rotor. The rotor is driven by a ½ hp, 2 pole, AC induction motor, and a v-belt pulley system (not shown). The electric motor is mounted on a pivot plate that allows for the tension in the belt to be varied. Figure 2 shows the system without the belts and the motor resting about 1 inch

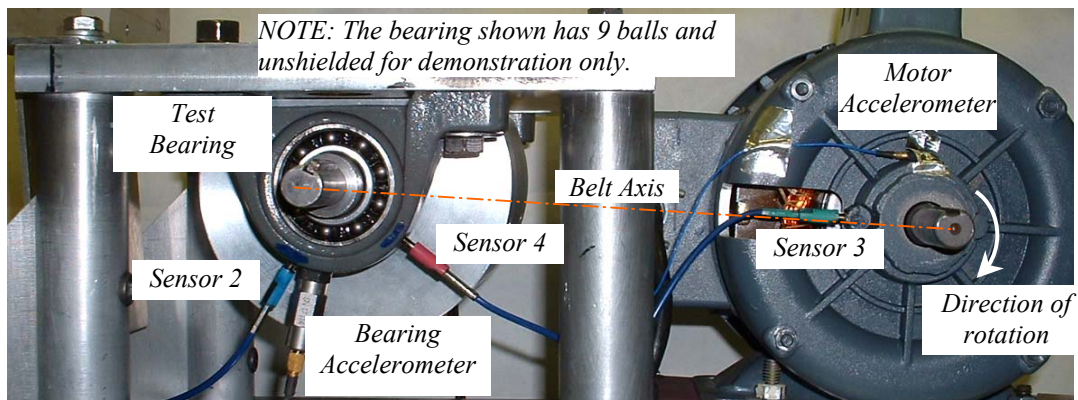


Figure 2: Test Set Up

lower than when the belt is on. The speed of the rotor is obtained using a magnetic proximity sensor that picks off of the key way (not shown). The pulley ratio is 1.38:1 and acts as a speed reducer.

The electric motor has both a *FOREST* sensor and an accelerometer located on the inboard bearing. The face of the motor was modified so that the *FOREST* sensor (*Sensor 3*) could be installed such that it would be in line with the belt axis between the two shafts. The modification was done strictly so that it can be demonstrated that the sensor is capable of acting within close proximity to the coils of the motor and to get radial access to the bearing. Installation of the sensor in an industrial environment would require a modified approach. Due to space constraints; the accelerometer is located 90 degrees clockwise from the sensor. This location also provides a flat area that can accommodate the mounting of the accelerometer.

The roller bearing has two *FOREST* sensors and one accelerometer. One *FOREST* sensor (*sensor 4*) is located within the loaded region of the bearing and is clocked 40° from the belt axis of the system. The second *FOREST* sensor (*sensor 2*) is located approximately 80° clock-wise from *sensor 4*. The accelerometer is located about 70° clock-wise from *sensor 4*. Adhesive mounts the accelerometer to the exterior of the bearing housing. Data from the accelerometers was obtained, but space and focus of this paper limited a full discussion of the comparison of the data between the *FOREST* sensors and accelerometers.

Data collection for the tests conducted incorporates a National Instruments DAQ system and a PC. Time waveforms and spectrums were obtained where needed.

The tests conducted to demonstrate the performance of the *FFPI* based sensor start with tests at speeds such that dynamic effects are negligible and then proceed to tests at operating speed. The tests with negligible dynamic effects are labeled as slow roll tests, *SRT*. These tests are conducted in three stages. The first stage is with the drive belt removed. These tests demonstrates the loading that each rolling element is experiencing due to the housing fit, shaft alignment, and rotor load. The second stage is with the drive belt attached with incremental loads on the pivot plate. The final test is conducted to show the ability of the *FOREST* sensor to respond to what is essentially a static change in loading of the system. The slow roll tests only require the time waveform to be acquired.

Test conducted at operating speed involve adding load to the pivot plate of the motor to increase the belt tension. These tests require both the time waveform and spectrum to be acquired.

The time waveforms, consisting of a series of peaks and valleys, depict the passage of the rolling elements past the *FOREST* sensor. The peaks represent instances when the sensor is highly loaded due to the rolling element pushing on the outer race and are directly in line with the sensor. The valleys represent instances when the sensor is located between two rolling elements. The sensors are initially preloaded to ensure contact between the tip of the sensor and the bottom of the sensor port. The trends reported are measured

relative to the preload so a negative load does not represent a change in load direction, but rather a reduction of the preload of the sensor. A reduction of preload also indicates that the outer race is pulling away from the sensor.

DATA: Slow Roll Tests: Bolt Loading:

The effect of mounting bolt loading the rolling elements is demonstrated by torquing the mounting bolts of the bearings housing in different stages. Three tests were conducted starting with all four bolts un-torqued, then proceeding by torquing bolts that are diagonal to each other, then ending with the torquing of the final two bolts, figure 3. The first test demonstrates the passage of the rolling elements with a rotor that is not overly constrained. The remaining tests demonstrate how torquing the mounting bolts can distort the bearing housing resulting in additional loading on the rolling elements. The load in the plots is that observed by the sensors. This information could be used to determine the distributed loading on the outer race of the bearing by use of either a finite element model or an elasticity-based model. Figure 3 shows the four mounting bolts and the order in which they were tightened. Case 1 is with all four bolts loose. Case 2 is with bolts 1 and 4 tightened. Case 3 is with the additional tightening of bolts 2 and 3.

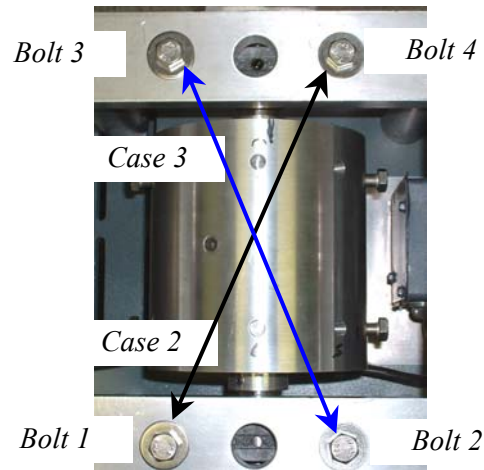


Figure 3: Bolt Pattern for Bearing Housings

Figure 4 shows the response of *sensor 4* to the three loading cases. Case 1 displays the lightly loaded condition of the rolling elements as the passage of each individual rolling element is not readily apparent. However, there does appear to be a strong *1X* component. The *1X* time trace is a reference to relate the trends for each of the three cases. Although care was taken to rotate the rotor at the same speed, 2 Hz, for all three cases, there may be small differences in rotor speed between the three cases. For this analysis, the small speed

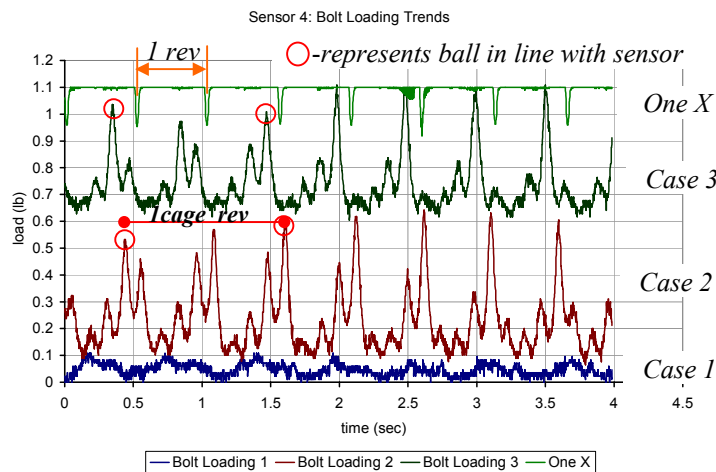


Figure 4 :Sensor 4 Response to Bolt Torquing

differences are not a factor as the overall loading observed by the sensor and resulting trends are more important. Case 2 shows that torquing bolts 1 and 4 load the bearing sufficiently so that the individual ball passage is more readily apparent. The tightening of the two bolts causes the rotor to become misaligned to some degree. Also, tightening of the bolts restricts the motion of the rotor causing any misalignment in the bearing elements to become more pronounced. The notable change in ball pass response is a clear indication that the housing is highly loaded in that direction. The pronounced ball passage can also be a result of the decrease in the clearances present in the bearing. Comparison to figure 5, which shows the responses of *sensor 2* for the three cases, shows

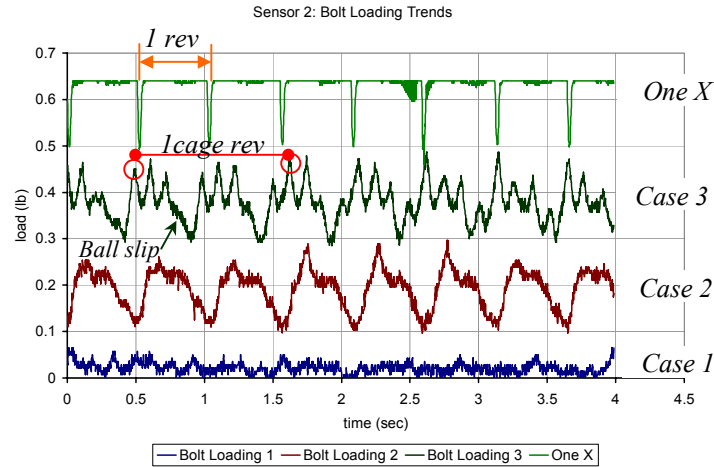


Figure 5: Sensor 2 Response to Bolt Torquing

a strong *1X* response, but a weak presentation of the individual ball passages for case 2. The final case shows that the overall peak response diminishes, but each plot shows that the ball passage response is somewhat uniform between the sensors. Table 1 summarizes the peak responses for the three cases.

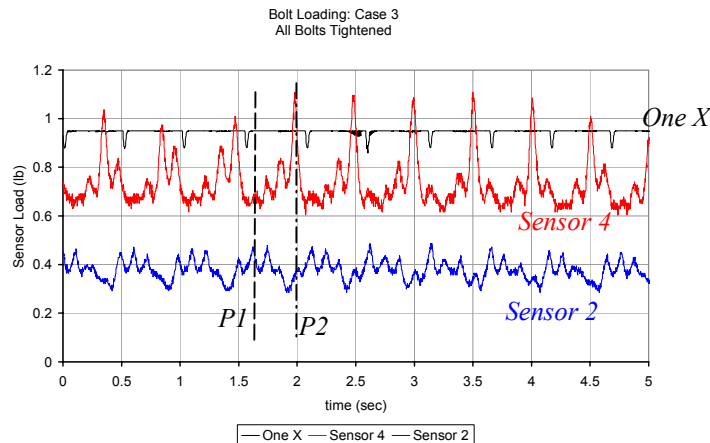


Figure 6: Slow Roll Response for all Bolts Torqued

Comparing the time trace for *sensors 2* and *4* for case 3 can extend the loading analysis. Two observations from the time traces shown in figure 6 is that two factors are most likely contributing to the uneven loading of the rolling elements. Working from the basis that if the shaft is aligned correctly, is not bent, and that the bearings are perfectly

aligned, each rolling element should display a similar loading and unloading response as it passes each sensor. This is not observed. The first observation is that the peak loading of each sensor is different in magnitude, and the second observation is that there is a loading that corresponds to shaft position. If static alignment was the only contributing factor, then the higher loading of the rolling elements would only occur in one direction and each rolling element would exert essentially the same amount of loading. However, from the time traces in figure 6, it can be observed that there is a high loading on one sensor. Then after the shaft has rotated around; the next sensor is highly loaded. This could be due to either a bent shaft or a cocked inner race. The reference line *P1* marks a point in time when *sensor 2* has high loading and *sensor 4* has a markedly reduced loading. This can be explained that the defect in the system is pushing on the shaft forcing it into *sensor 2* and essentially unloading *sensor 4*. Then, as the shaft rotates to the reference line *P2*, *sensor 4* is now highly loaded, and *sensor 2* is now unloaded. This cycle is then repeated for additional shaft rotations. There also exists to some degree a static mis-alignment too. This can be observed by the fact that the loading of *sensor 2* is essentially uniform for the peak and valleys for the ball passages, however, *sensor 4* shows that each ball passage has an increasing trend. If the shaft were misaligned in the direction of *sensor 4* then the balls in that direction would experience a higher loading than that observed by *sensor 2*. However, as the shaft rotation component of misalignment rotates around and becomes aligned with the misalignment in the direction of *sensor 4* a superposition of load occurs, resulting in a higher load. There is a modulation that occurs in the overall time waveform due to the difference between the shaft speed and cage rotational speed. This difference accounts for the fact that the rotating defect does not necessarily align with a ball and the sensor every time the defect passes the sensor.

Table 1
Sensor Peak Response to Bolt Tightening

	<i>Sensor 4</i> (lb)	<i>Sensor 2</i> (lb)
Case 1	0.108	0.05
Case 2	0.505	0.182
Case 3	0.467	0.177

Slow Roll Test: Belt Loading Again, the slow roll tests are conducted such that the speed of the rotor is around 2 Hz. The loading trends of each rolling element due to increased belt tension can be assessed from this type of test. The loading of the rolling elements is observed in figures 7 and 8. Due to the tension developed in the belt, the bearing is pulled into *sensor 4* causing the ball passage to be more pronounced. The trends also show that *sensor 4* observes a different loading than *sensor 2*. The ball passage is more apparent in the trend for *sensor 4* than in *sensor 2*. The relation of the travel of a rolling element requires an understanding of the angular spacing between the two sensors, 85°, and the angle between each rolling element, 36°. This would indicate that two rolling elements could be located between a ball passing *sensor 4* and *sensor 2*.

So, when “Ball 1” passes *sensor 4*, counting two balls on *sensor 2* time waveform will show “Ball 1” passing *sensor 2*. This can be observed in Figure 8. Selecting a peak and counting ten peaks will identify one cycle of the cage. Comparing the two time traces it is quite evident that the passage of the balls past each sensor is not uniform indicating that the bearing is misaligned. Note in these figures the large peaks that occur about every one revolution of the shaft. This is a strong indication that either the rotor, or a race of the bearing is misaligned

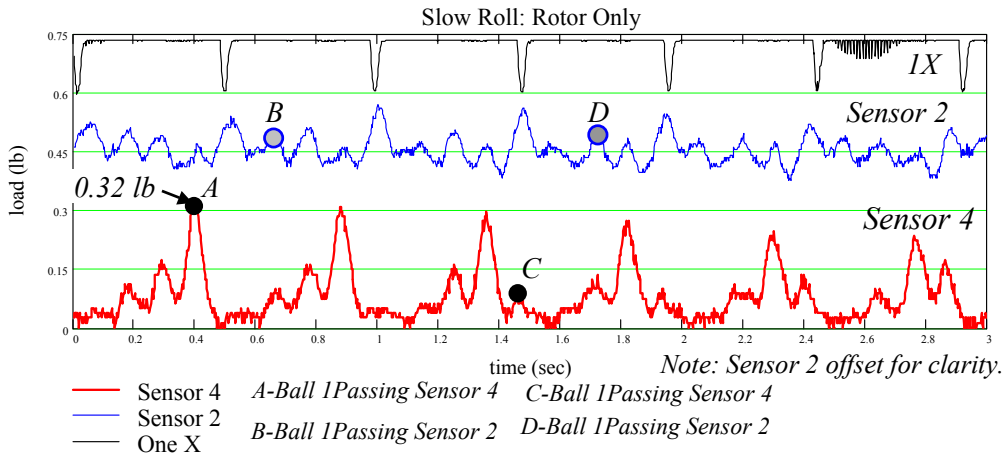


Figure 7: Time Waveform for Slow Roll of Rotor Only

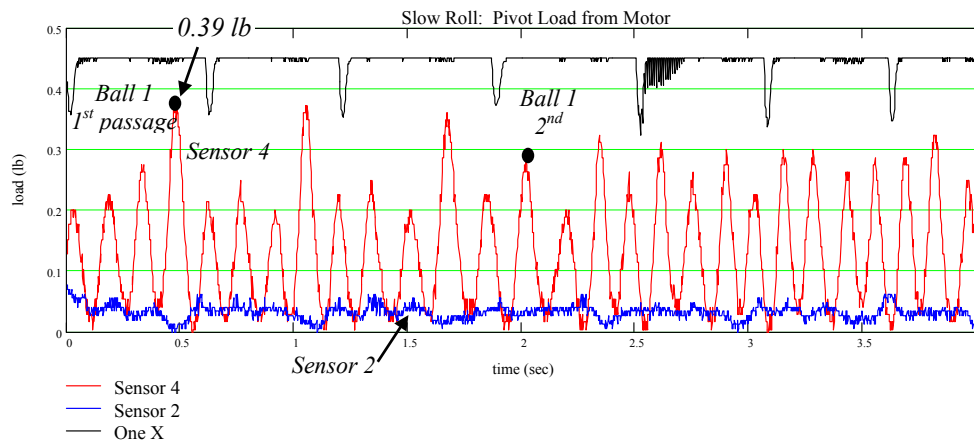


Figure 8: Time Waveform for Slow Roll of Loaded Rotor

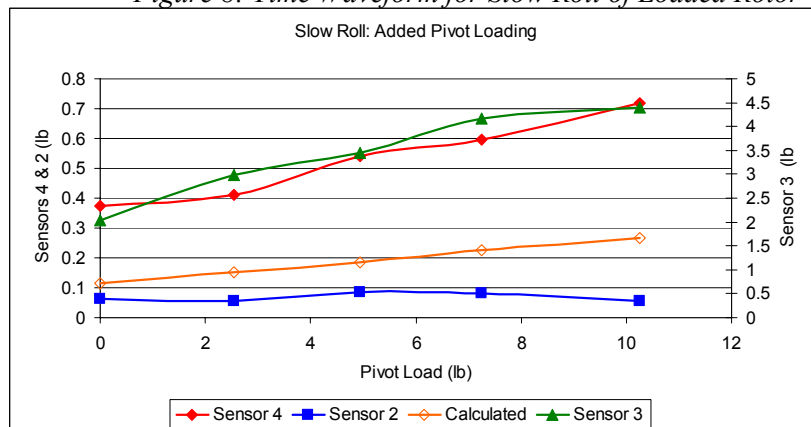


Figure 9: Time Waveform Maximum Peak Loads for Slow Roll

By increasing the belt load by applying weight to the pivot plate of the motor, it is expected that the ball pass on *sensor 4* will become more distinct and the loading of *sensor 2* would decrease. This is observed in figure 8 and is the result of the belt tension due to the weight of the electric motor on the pivot plate. This trace clearly shows the loading of the individual rolling elements passing *sensor 4*, and the unloading of *sensor 2*. The unloading of *sensor 2* occurs because the belt loading pulls the bearing away from *sensor 2*. Figure 9 shows the trends of the peak loading for an increase in the belt tension due to four uniform increases in load on the pivot plate for the motor. The result that is to be expected is that the peak load from the time waveforms should increase uniformly. This is observed. The trend of *sensor 2* also indicates that the unloading effect is steady for all loading conditions. The difference between the calculated loading and the actual loading of *sensor 4* is that the calculated value does not account for the interference fit and the misalignment. The loading for *sensor 3*, located in the electric motor, is higher than that for *sensor 4* because the interference fit for the bearing on the electric motor is tighter than for the bearing on the rotor and also because *sensor 3* is aligned with the belt axis, figure 2. Table 2 shows a comparison of the expected bearing loads in the direction of *sensors 3* and *4* respectively for both slow roll testing and for at speed tests. The loads stated in Table 2 represent values of loads acting on the inner race of the bearing. The values observed in the plots represent loads observed by the sensor. Transfer functions can be obtained to relate the load on the inner race to the observed load on the bearing. However, the transfer function is strongly dependent on the position of the ball with respect to the sensor. As an example, *sensor 4* has a transfer function of approximately $0.005 \{ \text{sensor load} / \text{inner race load} \}$ when the load on the shaft, a rolling element, and the sensor are aligned.

Table 2
Pivot Load and Estimated Bearing Loads (lbs)

Applied Pivot Load (lb)	Slow Roll Tests		At Speed Tests	
	Rotor Bearing Sensor 4*	Motor Bearing	Rotor Bearing Sensor 4*	Motor Bearing Sensor 3
0	22.6	35.2	53.4	83
2.54	30.2	47.1	61	94.1
4.54	37.3	58.1	68.1	105.1
7.25	45.1	70.2	75.9	118.1
10.25	53.1	82.8	83.4	130.5
*This is the load in the direction of <i>sensor 4</i> .				

At Speed Tests: Belt Loading Conducting the same loading tests on the pivot plate with the rotor running at speed, 42.5 Hz, should produce similar results as the *SRT*. The loading is expected to be higher due to the torque contribution the v-belt drive. The running speed tests also allow for the introduction of spectrums in the loading comparison. Figure 10 shows, at running speed, a time window of 0.15 seconds. The same loading trends are noticed as in the slow roll case but with increased peak loadings. Figure 11 shows a time window of 1.5 second. A definite modulation of the time waveform is observed. The modulation could be attributed to the belt and to the

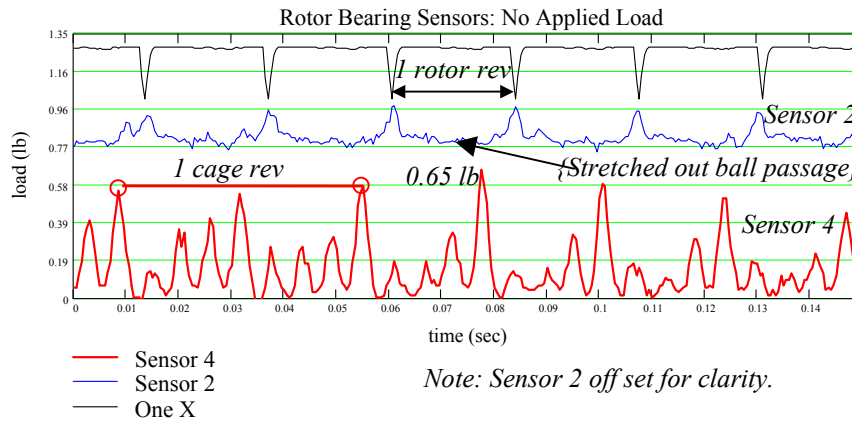


Figure 10: 0.15 sec. Ball Passage for Rotor Bearing at Running

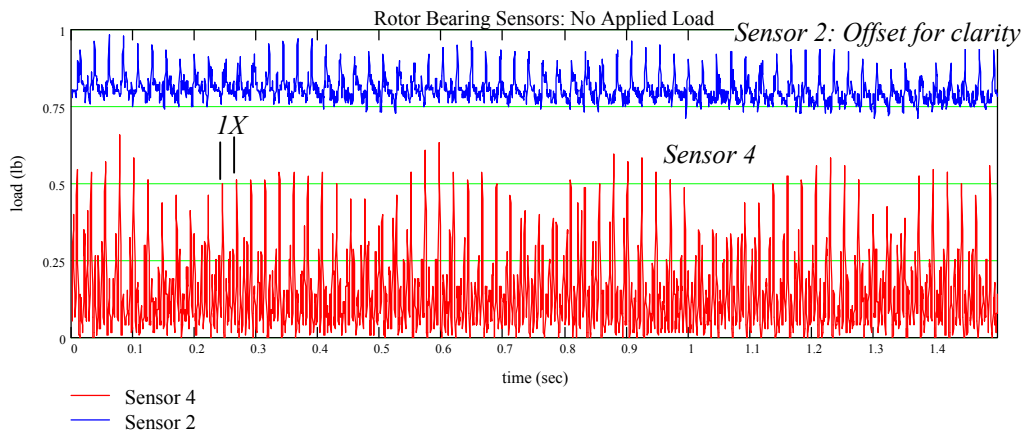


Figure 11: 1.5 sec. Time Waveform for Sensors 4 and 2

misalignment of the bearing. The cyclic loading is apparent; as is that some rolling element passages do not produce definable, or stretched out, peaks. A stretched out ball passage could be attributed to the ball sliding past the sensor, figure 10. The test shown here are for a rotor that is lightly loaded. The loading on the in-board bearing due to the heaviest load applied to the motor pivot plate at running speed is approximately 110 lbs, where as the lightest case is approximately 45 lbs. The radial load capacity for the test bearing is 170 lbs for an operating life of 30,000 hrs. This loading could fall under the lightly loaded category of a rotor. Figure 12 shows the resulting trends from increasing the load on the motor pivot plate by the same amounts as in the *SRT*. Again, a linear increase is observed in *sensors* 3 and 4, where as *sensor* 2 has a fairly steady response. A strong *1X* response is observable in figure 10 and figure 11. This response can be attributed to a combination of misalignment and looseness. The bearing insert has a very weak interference fit as it could be installed by hand. This looseness allows the outer race to essentially orbit in the housing that can generate a strong *1X* response.

The response of the *FOREST* sensor is dependent on the spacing between the mirrors. The gap between the mirrors can be influenced by thermal changes over time and results in a ramping effect of the signal. This phenomenon could lead to problems when trying to

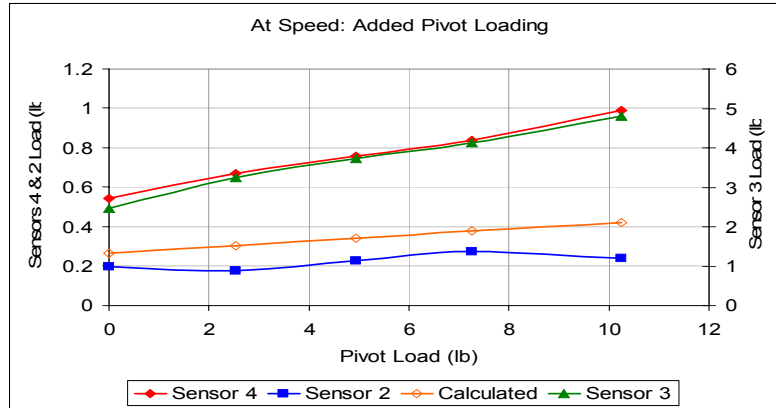


Figure 12: Trends of Peak Load Values from Time

trend the data due to load strictly using the time waveform. The trending problem can be aided by the use of spectrum analysis. Spectrum analysis requires an understanding of the possible frequency components that one would expect to see for a given system. For the time waveform shown in Figure 11 a spectrum is shown in Figure 13, which is typical for the *FOREST* sensor. Again, the no applied load case refers to the no load being applied to the motor pivot plate. The spectrum covers a range of 350 Hz. The boxed regions are shown in figures 14 and 15 displaying the information around the *IX*, rotor shaft speed, region and *outer ball pass*, *OBP*, region respectively. Figure 14 shows that there are very prominent frequencies that correspond to expected frequencies of the rotor, bearing, and belt. Figure 15 emphasizes the content of the spectrum in the vicinity of the outer ball pass frequencies. Comparing the magnitudes between figures 14 and 15 it can be observed that the outer ball pass is very dominant. The problem with trending spectrums is understanding what parts of the spectrums can be used to identify or trend the loading associated with an increase in drive load. Figures 16 and 17 show the resulting trends of a number of peaks from the spectrum plots for each of the *FOREST*

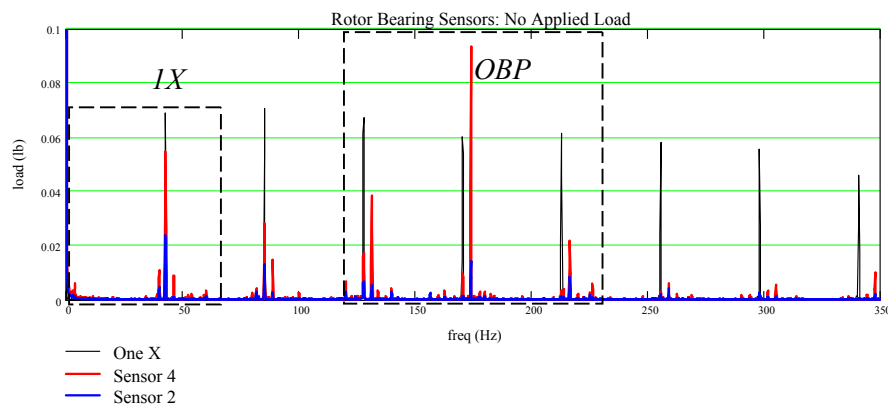


Figure 13: Spectrum for Time Waveform in Figure 7

sensors. Figure 16, *sensor 4*, shows that the *IX* and *OBP* frequencies both display a linear increasing trend of peak due to the increase in belt tension. Other frequencies that exhibit a tendency to increase according to applied pivot load are the *2X* and *2OBP*. Figure 17 represents the trending of the same frequency components for *sensor 2*. The trends again support the fact that the increased belt load is actually pulling the bearing

away from *sensor 2*. This is observed by the decrease in the *OBP* and *OBP-1X* frequencies. The trends of the *1X* and *2X* components show that there is a loading that causes the outer race to respond to the rotor motion. The fit of the outer race in the bearing housing can best be described as loose as the bearing insert could be installed by hand. This loose condition could allow the outer race to essentially orbit in the housing and respond strongly to a *1X* motion.

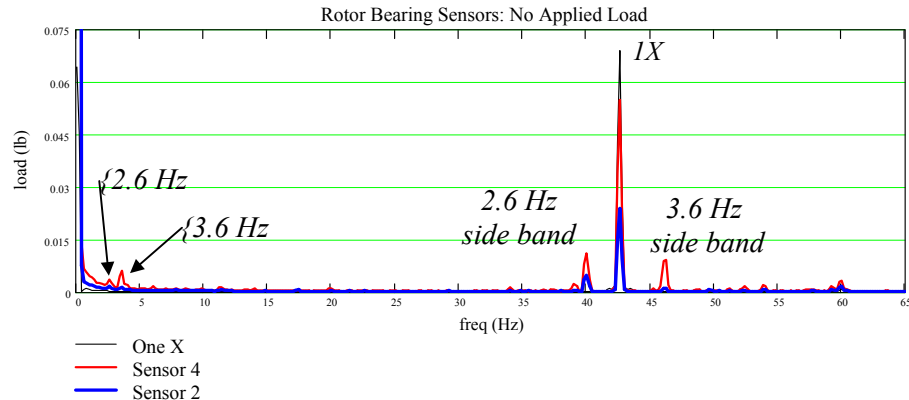


Figure 14 : Zoom on Spectrum 1X Region for figure 13

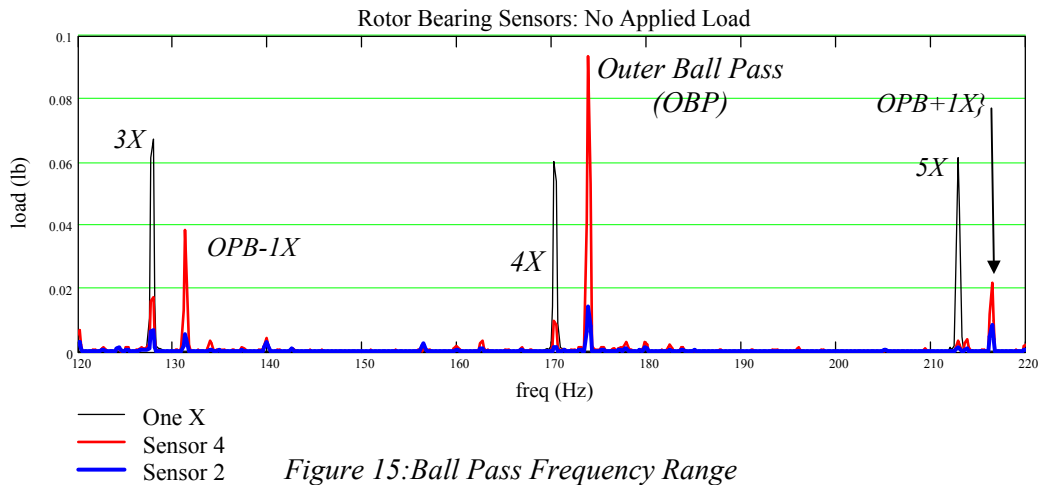


Figure 15: Ball Pass Frequency Range

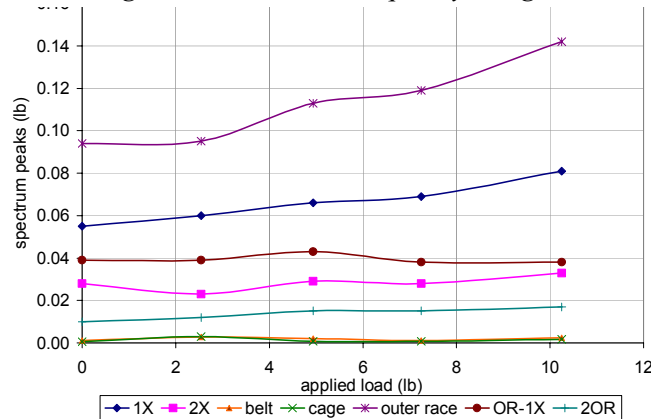


Figure 16: Trend of Spectrum Peaks for Sensor 4

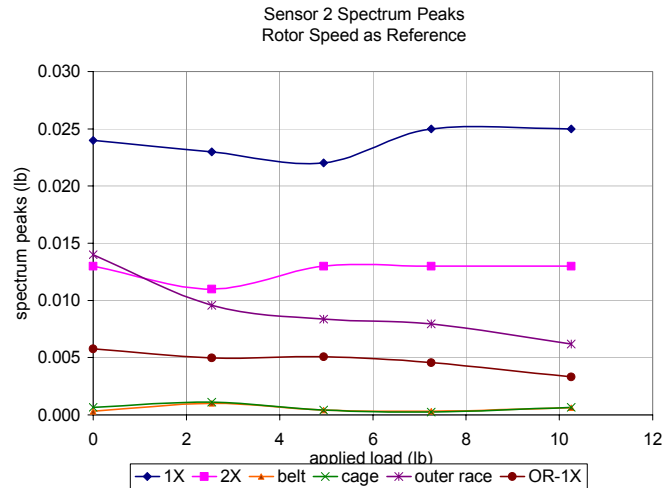


Figure 17: Trends of Spectrum Peaks for Sensor 2

Transient Loading: Time waveforms are useful when transient events occur. Figure 18 represents a time window when a load is applied to the pivot plate at about the 2-second time marker. The trend for *sensor 3* changes as a step function and the overall peak value increases by 1.53 pounds as observed by the sensor. The actual load on the bearing is at least 50 times greater than what the sensor observes when the transfer function is applied.

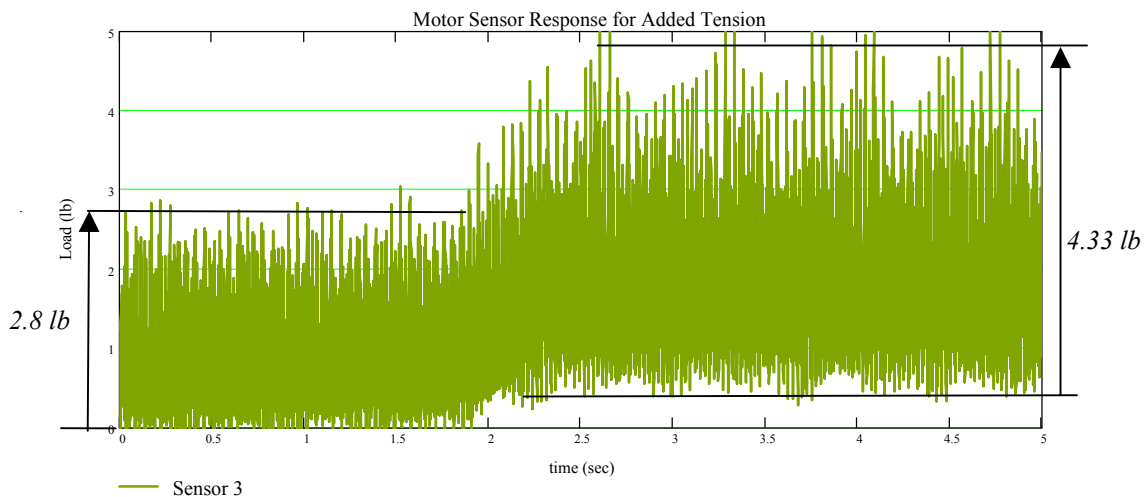


Figure 18: Sensor 3 (motor) Response to Applied Pivot Load

Summary: The *FOREST* sensor based on the Fiber Fabry Perot Interferometer (FFPI) is uniquely capable of providing information regarding the loads experienced by roller element bearings at both low and operating speeds. Additionally, the sensor does not require to be in direct contact with the outer race but can instead operate by making contact within the bearing housing with only a few mils of material between the outer race of the bearing and the probe tip. This allows for a stronger structure. Some other advantages over traditional transducers include high sensitivity (0.05 micro-strain), small

diameter (4.9 mils, 0.125 mm), immunity to EM fields, and continuous operation at high temperatures (450°C) .

Slow roll tests conducted with the *FOREST* sensor demonstrates its distinct ability to produce valuable static and “low speed” data, that can be attributed to interference fit, rotor dead load, misalignments, and drive pre-loads. The slow roll tests discussed in this paper showed the sensor was able to detect the load changes experienced by the bearings arising from installation and belt load changes.

Tests at operating speed were able to provide information relevant to the loading cycle of the bearing and rolling elements as well as information on the various frequency components. Individual spectrum frequencies arising from bearing components and the system can be used to trend various aspects of the loading of the bearing. The spectrums shown were relatively clean and contained spikes relevant to the system. This data can provide insight into the dynamic loads affecting a bearing arising from drive, process, and rotor loads.

Further studies are to be conducted to relate the response of the *FOREST* sensor to imbalance and defect detection. These studies are to be conducted so that a comparison can be made between the *FOREST* sensors and accelerometers. Although the tests shown here are for essentially short time durations, it is felt that the *FOREST* sensor is capable of providing information that could be usefully trended of long operation periods.

References

- [1] Jones, R. M., “Rolling Element Bearing Status Using Frequency Analysis”, Fluid Handling Systems, May 2000.
- [2] Zarestky, E.V., Poplawski, J.V., Miller, C.R., “Rolling Bearing Life Prediction –Past, Present, and Future”, NASA/TM-2000-210529.
- [3] Patrick, G., “New Technology-Same Old Problem”, Sound and Vibration, May 2002, 10-15.
- [4] Zarestky, E.V., *STLE Life Factors for Rolling Bearings*, STLE Publication SP-34, 1999.
- [5] Taylor, H.; “Fiber Fabry Perot Interferometer (FFPI) Sensors” 50th Annual Symposium on Instrumentation for the Process Industries, College Station TX, Jan. 1995.
- [6] Fiber Dynamics Incorporated web site. Brochures, <http://www.fiberdynamics.com>.
- [7] Atkins, R.A.; Lee, C; Taylor, H; “Fiber Optic In Cylinder Pressure Cylinder Developed”; Diesel & Gas Turbine Worldwide, 1995
- [8] Perez, R. X., Sampathkumar, V., Zeidan, F., “Force Sensing Fluid Film Bearing: New Vibration Monitoring”, Turbomachinery International, Vol. 43 No. 4, July/August 2002, pgs 18-21
- [9] Perez, R. X., Lee, C., Taylor, F, “Using Fiber Optic Pressure Sensors to Detect Cavitation and Instabilities in Pumps”; Pumping Technology, 1998.

- [10] Raymer, S. G.; Childs, D.W.; “Force Measurements in Magnetic Bearings Using Fiber Optic Strain Gauges”; Proceedings of ASME Turbo Expo 2001 . 2001-GT-0028; ASME Turbo 2001 June 4-7, 2001
 - [11] Yang, Y., Danyluk, S., “A Study on Rolling Element Skew Measurements in a Tapered Roller Bearing With a Specialized Capacitance Probe”, Journal of Tribology, Vol 122, July 2000, pp 534-538.
 - [12] Harker, R.G., Sandy, J.L., “Rolling Element Bearing Monitoring and Diagnostic Techniques”, Journal of Engineering for Gas Turbines and Power, April 1989, Vol 111 pp 251-256.
 - [13] Yu, J.J., Bently, D.E., Goldman, P., Dayton, K.P., Van Slyke, B.G., “Rolling Element Bearing Defect Detection and Diagnostics Using Displacement Transducers”, Proceedings of ASME Turbo 2001, June 4-7, 2001,
 - [14] Holm-Hansen, B.T., Gao, R.X., “Vibration Analysis of a Sensor-Integrated Ball Bearing”, Journal of Vibration and Acoustics, October 2000, Vol 122, pp 384-392.
 - [15] Philips, G. J., “ Bearing Performance Investigations Through Speed Ratio Measurements”, ASLE Transactions, Vol 22, 4, Oct 1979, pp.307-314.
 - [16] Philips, G.J. “ The Fiber Optic Bearing Monitor”; InTech Vol 29 No. 5, May 1982 pp. 43-45.
 - [17] Philips, G. J., “The Fiber Optic Bearing Monitor”, Instrumentation in the Aerospace Industry Vol 28, Advances in in Test Measurement-Vol 19 Part One, 1982 pp. 379-395.
- Other References
- [18] Brändlein, J, Eschmann, P., Hasbargen, L, Weigand K, *Ball and Roller Bearings, Theory, Design and Application* 3rd edition. John Wiley & Sons Ltd, 1999.
 - [19] Harris, T.A., *Rolling Bearing Analysis* 4th Edition John Wiley & Sons, Inc, 2001.
 - [20] Vance, J.M; “Rotordynamics of Turbomachinery”; 1988, John Wiley & Sons.